Influence of the Configuration of Consecutive Street Canyons and Atmospheric Stability

Byoungchull OH[1], Ryozo OOKA[2], Takeaki KATSUKI[3] and Hideki KIKUMOTO[1]

[1] Graduate Student, The University of Tokyo, Japan

[2] Professor, The University of Tokyo, Institute of Industrial Science, Japan

[3] Project Researcher, The University of Tokyo, Institute of Industrial Science, Japan

Abstract

This research, based on Computational Fluid Dynamics (CFD) analysis, focuses on the wind characteristics and the ventilation performance in the consecutive street canyons produced by various building complex configurations. In this research, the buildings in the street canyon space were distributed in either staggered or normal arrangements and, in consideration of the varying distribution and height of different buildings, high-rise buildings, middle-rise buildings and low-rise buildings were all included. The air flow field and concentration distribution change were compared at various degrees of atmospheric stability. In order to examine the ventilation efficiency and purging flow rate (PFR), 3 different atmospheric conditions were analyzed - a stable case, a weak-unstable case and an unstable case. Based on the analysis results, it was found that in isothermal cases the best pedestrian effect and ventilation efficiency were achieved when buildings with different heights were laid out in a normal arrangement. In non-isothermal cases, the highest ventilation efficiency was found in unstable conditions.

Keywords: CFD, Ventilation performance, Staggered arrangement, Normal arrangement, Atmospheric stability, Ventilation efficiency, PFR, Pedestrian effect

Introduction

Recently, the urban outdoor environment is worsening for air pollution by virtualization and urban congestion. For the purpose of improvement of air quality of urban area, it is necessary to enhance urban ventilation through and ventilation efficiency. In previous research, Yoshie et al. [1] carried out wind tunnel experiment under the conditions of variations of height of building and of gross building coverage ratio and gross floor-area ratio. Moreover, the effect of building height on the wind velocity and temperature at the pedestrian level was examined. The concept of ventilation in the vertical direction is introduced. Uehara et al. [2, 3] examined the flow field and the diffusion field under various the atmospheric stabilities in urban street canyon by wind tunnel experiments. Kim et al. [4] analyzed the influence of aspect ratio of the canyon space and surface temperature on airflow pattern and pollutant dispersion by CFD simulation. Furthermore, Hong et al. [5] examined the urban ventilation efficiency around an elevated highway by use of Visitation Frequency (VF) [6] and Purging Flow Rate (here after PFR) [7, 8] . However, the floor area ratio and the building coverage ratio are limited by legislations on an urban planning and a construction plans in the real urban. In these circumstances, it is difficult to obtain the general result of the ventilation efficiency.

In this study, it was assumed that several similar buildings were arranged in the mainstream direction and that a boundary layer was fully developed over the arrangement of street canyons. Four specific cases, each with a different type of building arrangement and height, were then compared at the same floor area ratio and building coverage-ratio in the same urban street canyon space. The pedestrian effect was evaluated in terms of the absolute wind velocity at pedestrian level, and ventilation was evaluated across a plane area at a standard height of 0.5H (7.5 [m]). CFD results were used to examine the pedestrian effect and ventilation efficiency in each case. Three additional cases, with different degrees of atmospheric stability, were also examined to investigate the influence of atmospheric stability on the flow pattern and the ventilation efficiency.

Description of CFD analysis

1. Analysis Cases

Fig.1 shows the analysis cases used in terms of their target area and Table 1 shows the floor area ratio, building coverage ratio and building size for each case. In Case 4, the building coverage ratio was a little smaller than the other cases. The [maximum] height of all cases was about 6.67H (100 [m]) in terms of computational area. The isothermal cases were

Case 1 to Case 4 and the non-isothermal cases were Case 5 to Case 7. The geometric parameters of the non-isothermal cases were the same as those used for Case 1.

2. Numerical conditions

Table 2 shows the governing equations used for CFD simulation. In this study, the standard k-ε model [9] was used as the turbulence model. Table 3 shows the analysis conditions and the boundary conditions. The first-order upwind scheme was used for the differential scheme of the convection term. A second-order central difference scheme was used for the other spatial finite differences. The generation condition of the pollutant was specified as 1 [μg m^{-3} s^{-1}] in the space from ground level up to a height of 0.5H. The transport of pollutant was assumed to be passive scalar. The temperature conditions are shown in Table 3. Table 4 shows the bulk Richardson number and temperature conditions of the non-isothermal cases.

Calculation of ventilation rate and PFR

In this study, ventilation efficiency was estimated from the interface-based ventilation rate and PFR of the target area of the canyon space, from ground level up to a height of 0.5H

(averaging the upper surface of the target area). Equation (1) and equation (2) show the interface-based ventilation rate and PFR.

$$Q[m^3 s^{-1}] = \int_V q dv / \frac{1}{S} \int_S C ds = q_p / Cs \quad (1)$$

$$PFR[m^3 s^{-1}] = \int_v q dv / \frac{1}{V} \int_v C dv = q_p / Cp \quad (2)$$

Here, q is the velocity of the pollutant generation rate per unit volume [μg $m^{-3}s^{-1}$], C is the pollutant concentration [μg m^{-3}], q_p is the velocity of the pollutant generation rate per unit time in the target area [μg s^{-1}], Cs is the horizontally averaged value of the concentration at the upper-interface of the target area [μg m^{-3}], and C_P is the spatially averaged value of the concentration in target area p [μg m^{-3}].

CFD results and discussion

In all the isothermal and non-isothermal cases, the absolute wind velocity, turbulent energy (k), temperature and the concentration of contaminant were examined in the vertical profile throughout the horizontal plane averaged across the target area.

1. Results for absolute wind velocity and turbulence energy, k

The profile of horizontally averaged absolute wind velocity

Fig. 2 and Fig. 3 show the profile of the horizontally averaged absolute wind velocity ($|\mathbf{U}| = \sqrt{U_1^2 + U_2^2 + U_3^2}$) in the isothermal cases and the non-isothermal cases, respectively. The absolute wind velocity in Case 1 was generally larger than the other cases, except near ground level in the canyon space. The absolute wind velocity of Case 2 was the smallest within the canyon space. In the upper region above the canyon, the absolute wind velocity in Case 1 was the largest, while the absolute wind velocity in Case 3 and Case 4 decreased because of the resistance of the high-rise buildings. From the viewpoint of the pedestrian effect, Case 3, which was composed of non-uniform building blocks, proved to be the most efficient. These results are very similar to those of Hagishima et al. [10]. By comparison, in the non-isothermal calculations, there was little difference between Cases 1, 5, 6, and 7 within the canyon space, from ground level up to a height of 1.0H (Fig. 3). In the upper region above the canyon, the absolute wind velocity in Case 1 (neutral) and Case 5 (stable) increased more than Case 6 (weak-unstable) and Case 7 (unstable). This was due to the turbulent kinetic energy and turbulent coefficient of viscosity in Case 6 and Case 7, increased by the buoyancy effect (as explained later). It was concluded that atmospheric stability does not have a great influence on the pedestrian effect.

The profile of horizontally averaged turbulent kinetic energy

The vertical profiles of horizontally averaged turbulent kinetic energy, k, in the isothermal and non-isothermal calculations are shown in Fig. 4 and Fig. 5. The turbulent kinetic energy in Case 3 was the largest and Case 4 was the smallest within the canyon space. Case 3 showed the largest value above a height of 1.0H and Case 4 showed the smallest. In the non-isothermal calculations, Case 7 (unstable) generally showed the largest value and Case 5 (stable) showed the smallest (see Fig. 5). This was due to atmospheric instability causing buoyancy production and increasing turbulent kinetic energy. The atmospheric instability increased the production term of turbulent energy by means of this buoyancy effect.

2. Results for temperature and concentration

The profile of horizontally averaged temperature

Fig. 6 shows the vertical profile of horizontally averaged temperature results for non-isothermal calculations. There was a very large vertical temperature difference within the canyon space in the unstable cases, while the vertical temperature gradients above the canyon were comparatively small.

The profile of horizontally averaged concentration

Fig. 7 shows the vertical profile of horizontally averaged concentration results for the isothermal calculations. Below a height of 1.0H, the concentration in Case 3 was the lowest

while the concentration in Case 4 was the highest. This is because the turbulent kinetic energy in Case 4 was small, and the turbulent mixing effect was not active. On the other hand, as the turbulent kinetic energy in Case 3 was large, the concentration decreased. Fig. 8 shows the results of the non-isothermal calculations. The concentration in Case 5 was larger than Case 1, whereas the concentration in Case 6 and Case 7 was smaller than Case 1. There was a clear relationship between atmospheric stability and concentration. This was due to the relationship between atmospheric stability and turbulent energy, i.e., the turbulence mixing effect illustrated in Fig. 5.

The interface-based ventilation rate and PFR per unit ground surface area

In order to analyze ventilation efficiency in the target area, the interface-based ventilation rate and PFR per unit ground surface area of the target area were compared. Here, the interface-based ventilation rate refers to the air exchange rate through the interface, as explained above. The height of the interface was set at 0.5H. Fig.9 shows the results of isothermal and non-isothermal calculations for the interface-based ventilation rate and PFR per unit ground surface area of the target area. These two indices showed the same overall trends, but the interface-based ventilation rate was a little larger than the PFR. This is because the averaged concentration of the interface

area was much lower than the averaged concentration of the canyon space. Based on the isothermal calculations, Case 3 showed the largest ventilation rate and Case 4 showed the smallest. In terms of the PFR, the results for Case 3 were also larger than Case 4.It can, therefore, be concluded that Case 3 produced the most efficient ventilation effect and Case 4 the worst. In terms of the interface-based ventilation rate, the results for Case 5 were smaller than Case 1, and the results for Case 7 were the largest, overall. Likewise, in terms of PFR per unit ground surface area, the results for Case 5 were also smaller than Case 1 and the results for Case 7 were the largest. In conclusion, it can be seen that atmospheric conditions had a significant effect on t he ventilation rate. Therefore, in this study, neutral atmospheric conditions (as shown by Case 1) produced a more efficient ventilation rate than stable conditions (Case 5) while unstable atmospheric conditions produced the most efficient ventilation rate of all. This is because the buoyancy effect, based on atmospheric stability, affects diffusion properties due to the turbulence mixing effect. The relationship between the bulk Richardson number (Rb) in the canyon space and the interface-based ventilation rate per unit ground surface area is shown in Fig. 10. As can be seen, atmospheric instability increased ventilation efficiency and atmospheric stability decreased ventilatin efficiency.

Conclusions

In this study, the ventilation efficiency within street canyons and the effects of wind on pedestrians were evaluated using CFD to compare various building configurations and arrangements. The following conclusions were obtained:

1. In the isothermal calculations, the horizontally averaged velocity in Case 1 (middle-rise buildings in a normal arrangement) was generally quite large within the street canyon. However, near the surface of the ground the velocity in Case 3 (high-rise and low-rise buildings in a normal arrangement) was the largest of all. Above the street canyon level, the horizontally averaged velocity in Case 3 and Case 4 (high-rise buildings in a normal arrangement) was quite small compared with the other cases tested.

2. In the non-isothermal calculations, there was very little difference between Case 1 (neutral), Case 5 (stable), Case 6 (weak-unstable), and Case 7 (unstable). Therefore, it was concluded that atmospheric stability has relatively little effect on wind at the pedestrian level.

3. In the isothermal calculations, the concentration in Case 2 (middle-rise buildings in a staggered arrangement) and Case 4 (high-rise buildings in a normal arrangement) was larger than that of Case 3 (non-uniform building height in a normal arrangement). This is because the non-uniformity of buildings caused a turbulence mixing effect. Therefore, the interface-based ventilation rate and PFR in Case 3 were relatively large.

4. In the non-isothermal calculations, the concentration in Case 5 (stable) was larger than Case 7 (unstable). This was a result of the unstable conditions generating turbulence due to the buoyancy effect and causing turbulent mixing. Therefore, the interface-based ventilation rate and PFR increased in proportion to the intensity of atmospheric instability.

References

1. Yoshie RYUICHIRO, Tanaka HIDEYUKI, Shirasawa TAICHI, Kobayashi TSUYOSHI : Experimental study on air ventilation in a built-up area with closely-packed high-rise buildings, *Journal of Environmental Engineering (Transaction of AIJ).* Vol. 73, No. 627, pp. 661-667. May 2008

2. Kiyoshi UEHARA, Shuzo MURAKAMI, Susumu OIKAI, Shinji WAKAMATSU : Wind tunnel experiments on how thermal stratification affects flows in and above urban street canyons, *Atmospheric Environment 34*, 1553-1562, 2000

3. Kiyoshi UEHARA, Shuzo MURAKAMI, Susumu OIKAI, Shinji WAKAMATSU : Wind tunnel test of concentration fields around street canyons within the stratified urban canyon layer, *J. Archit. Plann. Environ. Eng., AIJ*, No. 499, 9-16, Sep., 1997

4. Jae-Jin KIM, Jong-Jin KIM : A numerical study of thermal effects on flow and pollutant dispersion in urban street canyons, *Journal of Applied Meteorology*, 1999, Vol. 38 pp. 1249-1261

5. Hong HUANG, Shinsuke KATO, Ryozo OOKA, Taifeng JIANG : CFD Analysis of Ventilation Efficiency around an Elevated Highway using Visitation Frequency and Purging Flow Rate, *The Sixth Asia-Pacific Conference on Wind Engineering (APCWE-VI)*, pp.10, 2005.09

6. Csanady G. T. : Dispersal by randomly varying currents, *J. Fluid Mech.* Vol. 132, pp. 375-394, 1983

7. Sandberg, M. : The use of moments for ventilation assessing air quality in ventilated room, *Building Environ., 18*, 1983

8. Sandberg, M. : Ventilation effectiveness and purging flow rate - A review, ISRACVE ASHRAE, pp-17, 1992 *International Symposium on Room Air Convection and Ventilation Effectiveness, University of Tokyo,* pp. 1- 21, 1992

9. B. E. Launder, D. B Spalding : The Numerical computation of Turbulent Flows, *Computer Methods in Applied Mechanics and Engineering 3*, pp. 269 – 289, 1974

10. Aya HAGISHIMA, Jun TANIMOTO, Koji NAGAYAMA, Masahiro KOGA : Wind tunnel experiment on drag force coefficient of regular arrangement rectangular blocks with different heights, *Journal of Environmental Engineering (Transaction of AIJ)* , no. 619, pp. 39-46. Sept. 2007

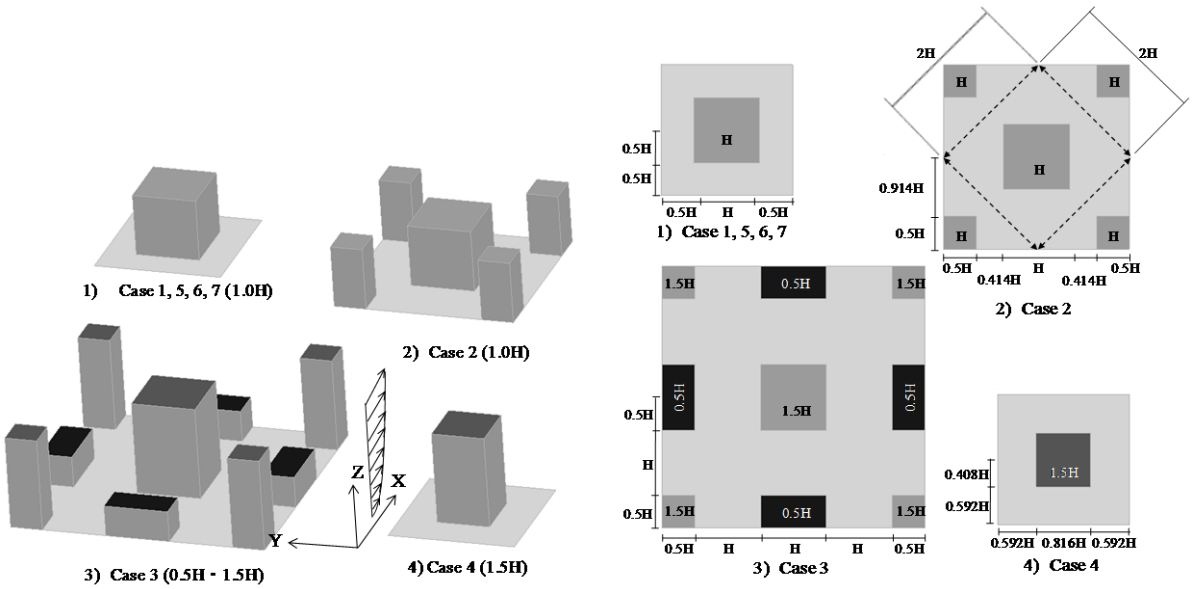

Fig. 1 Details of analysis cases showing target area (1.0H = 15 [m])

Table 1 Details of floor-area ratio, building coverage ratio, and building size

Case	Building size (X × Y × Z)	Building disposition	Floor-area ratio	Building coverage ratio
Case 1, 5, 6, 7	1.0H × 1.0H × 1.0H : Middle-rise	Normal arrangement	125%	25%
Case 2	1.0H × 1.0H × 1.0H : Middle-rise	Staggered arrangement	125%	25%
Case 3	1.0H × 1.0H × 1.5H : High-rise (Ⅰ)	Normal arrangement	125%	25%
	1.0H × 1.0H × 0.5H : Low-rise			
Case 4	0.816H × 0.816H × 1.5H : High-rise (Ⅱ)	Normal arrangement	125%	16.64%

1.0H = 15 [m]

Table 2 Governing equations for the k-ε two-equation turbulence model

$\frac{\partial U_i}{\partial X_i} = 0$	Continuity equation
$\frac{\partial U_i}{\partial t} + \frac{\partial U_i U_j}{\partial X_j} = -\frac{\partial}{\partial X_i}\left(\frac{P}{\rho} + \frac{2}{3}k\right) + \frac{\partial}{\partial X_j}\left\{\nu_t\left(\frac{\partial U_i}{\partial X_j} + \frac{\partial U_j}{\partial X_i}\right)\right\} - g\beta\Delta T\delta_{i3}$	Momentum equation
$\frac{\partial k}{\partial t} + \frac{\partial k U_j}{\partial X_j} = \frac{\partial}{\partial X_j}\left(\frac{\nu_t}{\sigma_1}\cdot\frac{\partial k}{\partial X_j}\right) + (P_k + G_k) - \varepsilon$	Turbulent energy transport equation
$\frac{\partial \varepsilon}{\partial t} + \frac{\partial \varepsilon U_j}{\partial X_j} = \frac{\partial}{\partial X_j}\left(\frac{\nu_t}{\sigma_2}\cdot\frac{\partial \varepsilon}{\partial X_j}\right) + \frac{\varepsilon}{k}(C_1 P_k + C_3 G_k) - C_2\frac{\varepsilon^2}{k}$	Turbulent dissipation rate equation
$\nu_t = C_\mu \frac{k^2}{\varepsilon}$	Equation for deciding ν_t
$P_k = \nu_t\left(\frac{\partial U_i}{\partial X_j} + \frac{\partial U_j}{\partial X_i}\right)\cdot\frac{\partial U_i}{\partial X_j}$	Production term for k
$G_k = -g\beta\frac{\nu_t}{\sigma_3}\cdot\frac{\partial T}{\partial X_i}\delta_{i3}$	Buoyant production term
$\frac{\partial \Phi}{\partial t} + \frac{\partial \Phi U_j}{\partial X_j} = \frac{\partial}{\partial X_j}\left(\frac{\nu_t}{\sigma_3}\cdot\frac{\partial \Phi}{\partial X_j}\right)$	Scalar transport equation

Here σ_1 = 1.0, σ_2 = 1.3, σ_3 = 1.0,

C_μ = 0.09, C_1 = 1.44, C_2 = 1.92, $C_3 = C_1 (G_K > 0)$ or $C_3 = 0 (G_K \leqq 0)$

Where U_i is the mean of the velocity components in the x (i = 1), y (i = 2), and z (i = 3) directions, respectively. P is the mean static pressure, ρ is the air density, ν_t is the turbulent eddy viscosity, k is the turbulent kinetic energy, ε is the turbulent kinetic energy dissipation rate, g is the gravitational acceleration, β is the thermal expansion coefficient of air, δ_{ij} is the Krönecker delta, and Φ is the scalar such as temperature and concentration.

Table 3 CFD analysis conditions and boundary conditions

	Wind velocity	k	ε	Concentration	Temperature
Sky	$\frac{\partial U_1}{\partial X_3} = 0$, $\frac{\partial U_2}{\partial X_3} = 0$, $U_3 = 0$	$\frac{\partial k}{\partial X_3} = 0$	$\frac{\partial \varepsilon}{\partial X_3} = 0$	C = 0	T = 30 [℃]
Side	$\frac{\partial U_1}{\partial X_2} = 0$, $U_2 = 0$, $\frac{\partial U_3}{\partial X_2} = 0$	$\frac{\partial k}{\partial X_2} = 0$	$\frac{\partial \varepsilon}{\partial X_2} = 0$	$\frac{\partial C}{\partial X_2} = 0$	$\frac{\partial T}{\partial X_2} = 0$
Inlet	Cyclic ($\Delta p/\Delta x$) = 0.008/30 [Pa m^{-1}]	Cyclic			
Outlet					
Ground surface	Z_0 log low (Z_0 = 0.01 [m])	$\frac{\partial k}{\partial X_3} = 0$	$\frac{\partial \varepsilon}{\partial X_3} = 0$	$\frac{\partial C}{\partial X_3} = 0$	T = 29 [℃] (stable) T = 35 [℃] (weak-unstable) T = 40 [℃] (unstable)
Surface		$\frac{\partial k}{\partial Xn} = 0$	$\frac{\partial \varepsilon}{\partial Xn} = 0$	$\frac{\partial C}{\partial X_3} = 0$	

Xn: Vertical direction on wall surface

Table 4. Atmospheric stability and bulk Richardson number for different cases

Case	Atmospheric stability	Atmospheric Temperature [℃] : T	Surface Temperature [℃] : Ts	*Rb*
Case 1	Neutral	30		0
Case 5	Stable	30	29	0.0444
Case 6	Weak- unstable	30	35	-0.3171
Case 7	Unstable	30	40	-0.6511

bulk Richardson number $Rb = gH(T_H - T_S) / \{T + 273) (U_H)^2\}$

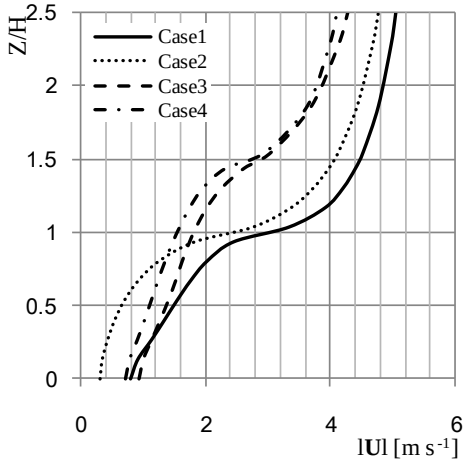

Fig. 2 Vertical profile of horizontally averaged absolute wind velocity (|**U**|) for isothermal cases

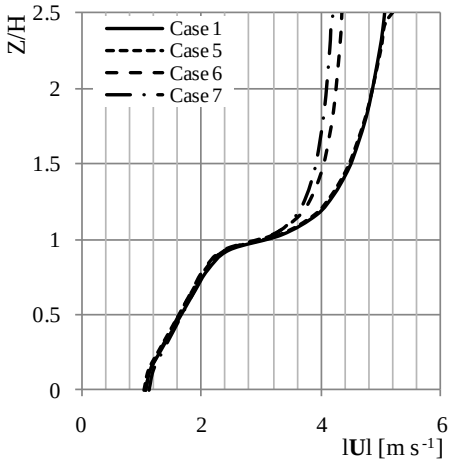

Fig. 3 Vertical profile of horizontally averaged absolute wind velocity (|**U**|) for non-isothermal cases

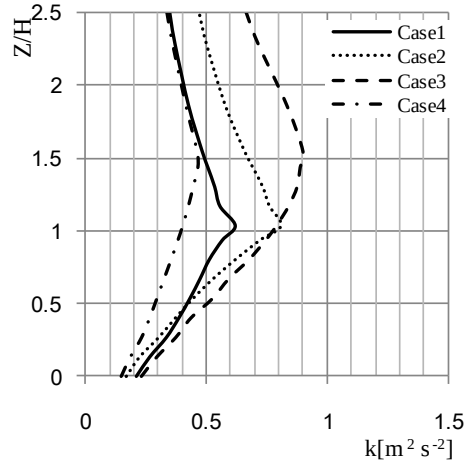

Fig. 4 Vertical profile of horizontally averaged turbulent kinetic energy

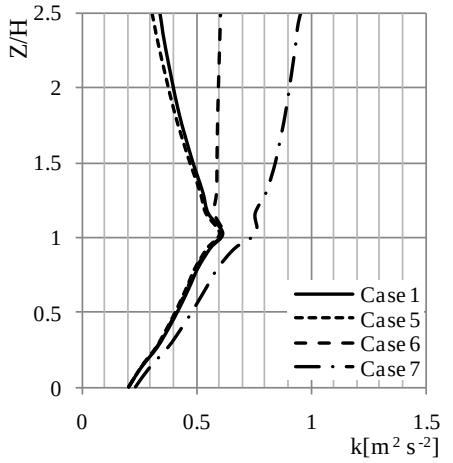

Fig. 5 Vertical profile of horizontally averaged turbulent kinetic energy

for isothermal cases for non-isothermal cases

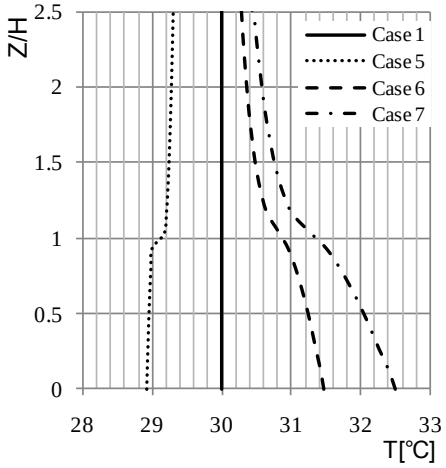

Fig. 6 Vertical profile of horizontally averaged temperature for non-isothermal cases the horizontal plane mean

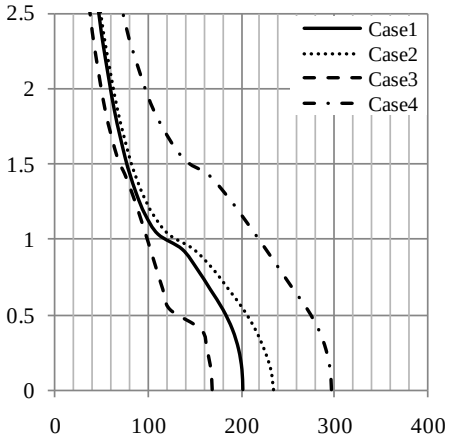

Fig. 7 Vertical profile of horizontally averaged concentration for isothermal cases

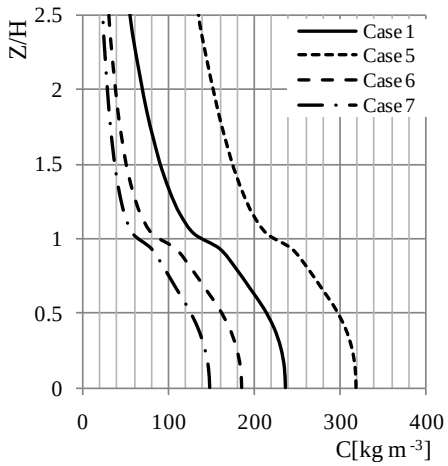

Fig. 8 Vertical profile of horizontally averaged concentration for non-isothermal cases

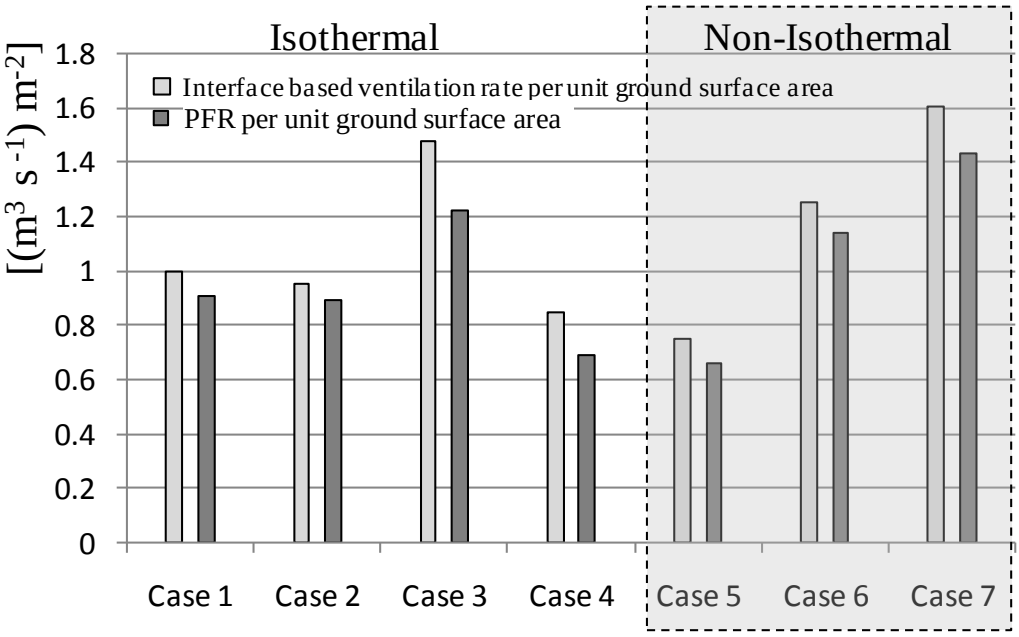

Fig. 9 Interface-based ventilation rate and PFR per unit ground surface area

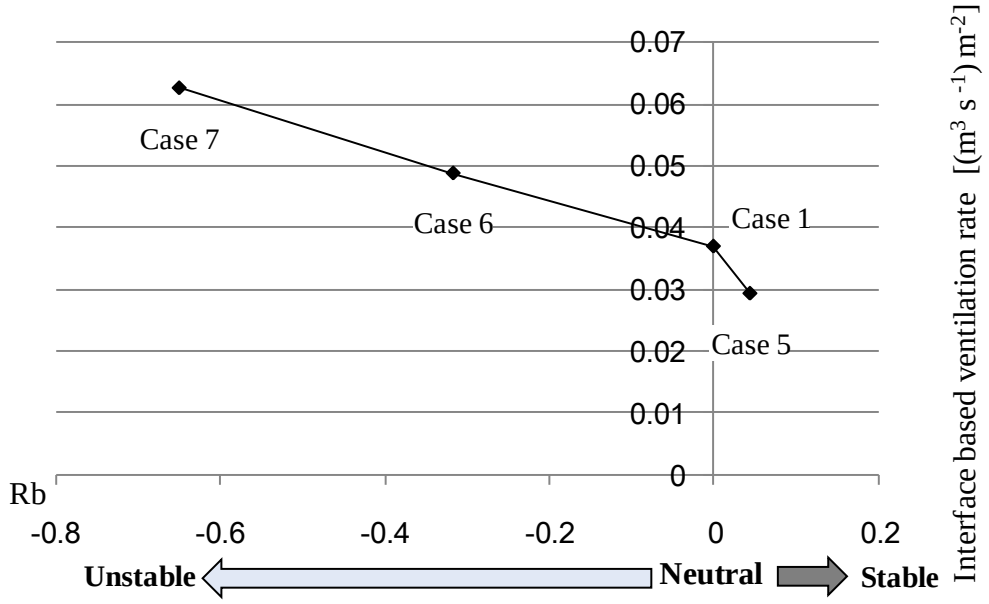

Fig. 10 Rb and interface-based ventilation rate per unit ground surface area